PCCP

Understanding the Vapochromic Response of Mixed Copper(I) Iodide/Silver(I) Iodide Nanoparticles toward Dimethyl Sulfide

Journal:	*Physical Chemistry Chemical Physics*
Manuscript ID	CP-ART-01-2020-000504.R1
Article Type:	Paper
Date Submitted by the Author:	02-Apr-2020
Complete List of Authors:	Nicholas, Aaron; University of Maine, Chemistry Barnes, Francis; University of Maine, Chemistry Adams, Daniel; University of Maine, Chemistry Webber, Matthew; University of Maine, Chemistry Sturner, Matthew; College of William & Mary, Chemistry Department Kessler, Matthew; College of William & Mary, Chemistry Department Welch, David; Suffolk County Community College Pike, Robert; College of William & Mary, Chemistry Department Patterson, Howard; University of Maine, Chemistry

Understanding the Vapochromic Response of Mixed Copper(I) Iodide/Silver(I) Iodide Nanoparticles toward Dimethyl Sulfide

Aaron D. Nicholas,[1*] Francis H. Barnes,[1] Daniel R. Adams,[1] Matthew S. Webber,[1] Matthew A. Sturner,[2] Matthew D. Kessler,[2] David A. Welch,[3] Robert D. Pike,[2*] and Howard H. Patterson[1]

[1]Department of Chemistry, University of Maine, Orono, ME 04469, [2]Department of Chemistry, College of William and Mary, Williamsburg, VA 23187, [3]Department of Physical Sciences, Suffolk County Community College, Selden, NY 11784

KEYWORDS. Chemical Sensors; Vapochromism; Nanoparticles; Copper Iodide; Luminescence

ABSTRACT: We report on the vapochromic behavior of a series of homo- and heterometallic copper(I) iodide/silver(I) iodide nanoparticles when exposed to dimethyl sulfide (DMS) vapor. These systems show remarkable colorimetric sensing behavior via emission color upon DMS exposure, shifting from pink to green emission. Kinetics measurements of CuI/AgI nanoparticle reactions with DMS show a significant increase rate increase with increasing Ag(I) content. However, luminescence spectroscopy and X-ray diffraction of the post-exposure samples with varying Ag(I) content reveal that the luminophore is identical in all cases and contains no Ag(I) ions. To rationalize the experimental observations and determine the vapochromic response mechanism, Molecular Dynamic calculations were performed on model (111) cation-terminated surfaces of copper iodide crystals doped with variable amounts of silver. Computational studies indicate that heterometallic Cu/Ag systems have a stronger binding affinity towards DMS vapor molecules than homometallic CuI and that embedding of the DMS molecules into the surface is the primary intermediate by which the vapochromic response occurs.

INTRODUCTION

Metal ions of the d^{10} group continue to attract interest from experimental and theoretical scientists due to their tendency to form self-assembled supramolecular and coordination polymers exhibiting metal-metal interactions.[1–15] These interactions produce strong light emission upon irradiation with UV light whereby the emission color is dependent on a number of physical properties such as coordinated ligands.[16–19] As a result, d^{10} metal-based materials have found applications as biosensors, optical sensors, and chemical sensors.[16,20–22] In many of these chemical sensor materials, the sensing potential of d^{10} metal-based systems is inherent to a well-documented, yet poorly understood, phenomenon known as vapochromism.[23-42] In this process the luminescence of a particular complex is altered by the presence of a volatile organic compound (VOC). We have observed this behavior previously with CuI films reacting to sulfur and nitrogen containing vapors, Scheme 1.[16] These films are generally non-luminescent under UV light but upon exposure to sulfur- or nitrogen-containing nucleophile vapors undergo a dramatic change in emission color, spanning the entire visible spectrum. While the metal halide film itself does not discriminate between incoming vapor molecules, the emission color is intrinsic to the particular molecule coordinated. The broad array of emission colors observed upon exposure to VOC vapors offers a proof-of-concept for the use of d^{10} metal halides in the development of chemical sensor devices. Nevertheless, through our study of CuI films, we identified that a major drawback to these systems is their limited ability to rapidly detect VOC vapors on the seconds time scale.

To overcome these reaction rate limitations, we have turned to mixed metal halide nanoparticle systems. Our approach was inspired by the recently published work of Leznoff *et al.* on Cu(I)/Au(I) cyano-coordination polymers, which demonstrated that heterometallic systems can be tuned to increase vapochromic response.[22,32,43,44] Amongst these systems, the vapochromic behavior of mixed metal $[Cu_{1/2}Au_{1/2}]CN$ towards thioethers is of particular interest.[22] When crystals of formula $[Cu_{1/2}Au_{1/2}]CN$ are prepared using equal molar ratios of metal ions, no vapochromic response is reported upon exposure to dimethyl sulfide or diethyl sulfide vapors. However, addition of excess Cu(I) during synthesis to form the 2:1 molar ratio compound $[Cu_{2/3}Au_{1/3}]CN$ activates the vapochromic behavior in which the emission shifts from blue to yellow. Given the isomorphic structures of the two metal cyanide salts, Leznoff *et al.* rationalized that the most likely cause of this behavioral change was disruption of stabilizing aurophilic bonding via Au(I) ion replacement by Cu(I). While it was determined via powder X-ray diffraction (PXRD) that binding of vapor molecules occurs only at Cu(I) sites in the final product, the mechanism by which this reaction proceeds is currently unknown. These findings highlight the need for fundamental mechanistic understanding of how vapochromic materials react with incoming VOCs as part of the rational development of commercially viable sensing materials.

To this end, we report on the synthesis and vapochromic response of a series of homo- and heterometallic CuI/AgI nanoparticles towards dimethyl sulfide (DMS) vapor. As noted, these nanoparticles display vapochromic behavior upon exposure to VOC vapor as evidenced by a distinct shift in emission energy. PXRD and luminescence measurements performed on

Scheme 1. Visible light photos of previously reported CuI films from our group under 365 nm irradiation after exposure to various VOC vapors.[16]

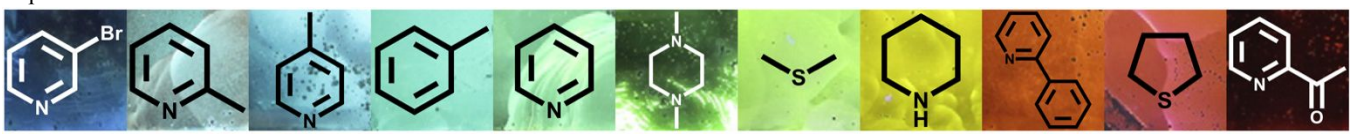

nanoparticles before and after DMS exposure showed that Ag(I) ions are not associated with the final emissive product. Most remarkably, in comparison to homometallic Cu(I) samples, nanoparticles with high Ag(I) content display far more rapid reaction times, with material saturation occurring within seconds. Molecular Dynamics calculations and kinetic studies have enabled us to develop a mechanistic understanding of how this vapochromic response occurs. To our knowledge this is the first study to probe the mechanism of nucleophile reaction with heterometallic iodide systems. Therefore, the current study represents the first structural, computational, and kinetic investigation into the vapochromic response mechanism of homometallic and heterometallic d^{10} metal halide building blocks.

EXPERIMENTAL

General. All reagents were purchased from Aldrich (St. Louis, MO, USA), Acros (Geel, Antwerp, Belgium), or American Element (Los Angeles, CA, USA) and were used as received. Diffuse reflectance spectra were collected on solid samples at 298 K. The light source was a Mikropack DH-2000 deuterium and halogen light source coupled with an Ocean Optics USB4000 detector. Scattered light was collected with a fiber optic cable. Spectra were referenced with $MgSO_4$. Data was processed using SpectraSuite 1.4.2_09. Compounds were analyzed for their Cu and Ag content via flame atomic absorption spectroscopy (AAS) using a Perkin Elmer AAnalyst 700 instrument. Samples were dissolved in 1.5 M aq. KI solution and then further diluted with water to a concentration of approx. 4.000 mg/L. All samples were measured three times with a reported average value. TEM services were performed by the University of Maine Electron Microscopy Laboratory. A Philips/FEI CM 10 TEM was used with a point resolution of 0.5 nm and lattice resolution of 0.3 nm. Magnification power in the range of 25× to 450,000× with an accelerating potential of 100 kV was used. For imaging, nanoparticles were deposited from sample solutions onto copper TEM grids coated with a layer of amorphous carbon. To deposit nanoparticles a small drop of nanoparticle solution was pipetted onto a grid surface and allowed to air dry at ambient temperature. Steady-state luminescence scans of unexposed and exposed nanoparticles were collected at 298 K. Spectra were collected with a Model Quantamaster-1046 photoluminescence spectrophotometer from Photon Technology International using a 75 W xenon arc lamp combined with two excitation monochromators and one emission monochromator. A photomultiplier tube at 800 V was used as the emission detector. The solid samples were mounted on a copper plate using non-emitting copper-dust high vacuum grease. Thermogravimetric analyses (TGA) were conducted using a TA Instruments Q500 in the dynamic (variable temp.) mode with a maximum heating rate of 50 °C/min. to 800 °C under 60 mL/min. N_2 flow.

Nanoparticle Synthesis. To synthesize CuI nanoparticles (**1**), CuI (0.800 mmol) was added to 20 mL aqueous solution of 3.0 M potassium iodide (KI). While stirring, 5 mL ethyl alcohol and 15 mL acetonitrile were added. The solution was vigorously stirred until no solids were observed. Under continuous stirring, excess deionized water was added drop-wise at a rate of 1 drop every 5 seconds until a precipitate was observed. An off-white powder was isolated by centrifuge and washed twice with water and once with ethyl alcohol. Nanoparticles were allowed to air dry overnight at room temperature. Measured AAS Cu content = 32.8% (theoretical = 33.4%). For $Cu_{0.80}Ag_{0.20}I$ nanoparticles, (**2**) the procedure described for CuI was followed using CuI (0.600 mmol) and AgI (0.200 mmol). A pale-yellow powder was isolated. Measured AAS Cu/Ag content = 23.8%/10.9% (theoretical = 25.5%/10.8%). For $Cu_{0.50}Ag_{0.50}I$ nanoparticles, (**3**) the procedure described for CuI was followed using CuI (0.400 mmol) and AgI (0.400 mmol). A yellow powder was isolated. Measured AAS Cu/Ag content = 14.4%/25.7% (theoretical = 15.0%/25.2%).

X-ray Studies. All powder diffraction measurements were collected on a Thermo Scientific ARL Equinox 100 instrument using a Co microfocus X-ray source at 45 kV, 0.3 mA. Powder samples were ground and placed into a spinning sample holder for analysis. Data in the range 5−110° 2θ were simultaneously acquired. The data were converted to Cu 2θ values from d-spacing according to Bragg's Law. Simulated powder patterns from single crystal determinations were generated using Mercury.[45]

Kinetic Measurements. Kinetic studies were performed by exposing 2 mg of nanoparticles to a mixed gas containing a controlled amount of nucleophile. To produce this mixed vapor with the target compound, air was bubbled through a liquid sample of DMS at 298 K. This saturated vapor was then mixed in a 1:1 ratio with air to reduce the concentration, producing the final experimental vapor. The flow rate was adjusted to 43.3 μmol hr^{-1} or 86.7 μmol hr^{-1} after which the system was purged 5 min to reach equilibrium. After 5 min the valve was closed, and nanoparticles applied on a glass slide were placed directly under the outflow. To measure the luminescence, a 350 nm mercury lamp was used as an excitation source and the emission was collected via a fiber optic cable. An Ocean Optics spectrometer was used as the detector. A dark spectrum was taken as a blank. Time acquisition measurements at specific wavelengths were taken until no change in emission intensity was observed. Three trials were collected and the data averaged.

Molecular Dynamics Simulations. Molecular Dynamics (MD) calculations were performed with the NANIM simulation program.[46] MD simulations were performed in the *NVT* ensemble with a time step of 2 fs, an equilibration period of 100 ps, and a production period of 100 ps. The temperature was set to 298 K via the velocity-rescaling thermostat (coefficient = 0.01 ps).[47] Each simulation was performed four times with statistical results averaged. Surface slab generation was performed using the zinc blende structure for copper iodide (assuming a lattice parameter of 0.620 nm). For pure copper iodide (case A), the slab has two-dimensional periodicity with dimensions of 5.2609 nm across the terrace and 5.3127 nm across the step. The slab depth is ~5.1 nm, with the top layer being a (111) face made up of cations and the bottom layer being a (111) face made up of anions. To perform silver doping at either ~25% (case B) or ~50% (case C) levels, each copper ion site in the slab was assigned, respectively, either a 1:4 or 1:2 chance of being replaced with a silver ion. As a result of the increase in lattice parameter caused by silver doping, slab dimensions for case B were increased to 5.3029 and 5.3551 nm (*i.e.* along periodic directions), and slab dimensions for case C were increased to 5.3448 and 5.3975 nm. To create a terrace along the cation-terminated surface at the top of the slab, one ~2.3 nm wide layer of metal-iodide pairs was removed (see Figure 1). Along this surface, sixty-three DMS molecules were distributed in order to obtain a monolayer (*note:* this amount of DMS was chosen because greater amounts resulted in significant desorption, creating an artificial vapor pressure in the simulation box). Two stationary walls confine this system along the non-periodic dimension. One wall (wall A) was placed well above the DMS monolayer, essentially serving as a top to the system. A second wall (wall B) was placed underneath the (111) anion-terminated surface of the slab, essentially acting as a substrate that supports the slab. After system construction, a force relaxation was performed over all non-copper atoms for 800 cycles in order to eliminate any artificially large forces that may be created due to rough atom placement.[46]

The atomic interaction model consists of Coulombic, Lennard-Jones, and Vashishta-Rahman interactions for the intermolecular potential and harmonic stretching/bending terms for the intramolecular potential.[48–54] Interactions between copper, silver, and iodide ions were treated with the approach of Vashishta and Rahman (*note*: the effective charges assigned in this model are +0.6 for Cu/Ag and –0.6 for I).[48] Repulsive, non-electrostatic interactions between metal cations were assumed to be negligible and were thus not included in simulations. DMS molecules were modeled according to the work of Bentenitis, Cox, and Smith.[49] Additionally, the force constants for intramolecular bond stretching and angle bending of the DMS molecule were taken from the AMBER 95 force field.[50] To determine the DMS-substrate interaction parameters, 12-6 Lennard-Jones potential terms for silver and copper atoms proposed in the work of Heinz *et al.* were mixed with those of the aforementioned DMS model by taking geometric means for ε and σ terms.[51] To determine a complete set of interaction parameters, a carbon-iodide interaction term was also taken from the literature and mixed with the DMS model.[52] Non-electrostatic interactions generally have a cutoff distance of 10 Å applied, except for the relatively long-range polarization interaction terms (used to describe part of the Cu-I, Ag-I, and I-I interactions) which have a larger cutoff distance of 20 Å applied. All intermolecular interactions discussed were treated with the shifted-force approach.[53] Coulombic interactions were modeled through shifted-force electrostatics with a cutoff distance of 20 Å applied.[54]

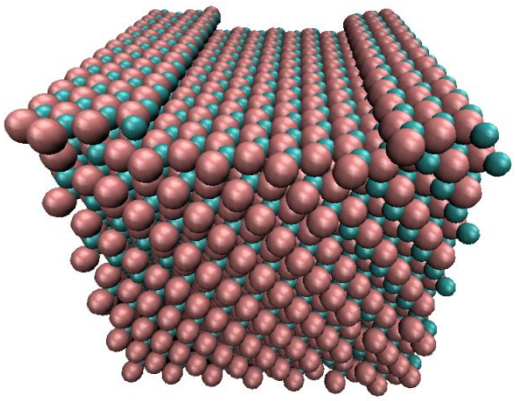

Figure 1. Substrate slab model. A homometallic (111) slab consisting of 2436 cation sites and two surface steps is constructed in order to assess the interaction of DMS molecules with copper iodide substrates. (Image made with VMD.[55])

The system walls act on nearby atoms according to a shifted-force 9-3 Lennard-Jones potential, using a cutoff distance of 10 Å.[53,56] This potential consists of a repulsive term, A/r_z^9, and an attractive term, B/r_z^3, where r_z is the vertical distance of the atom from the wall. Wall A has potential parameters of A = 180.83 eV/Å^9 and B = 0.78918 eV/Å^3, and wall B has potential parameters of A = 901.14 eV/Å^9 and B = 3.9328 eV/Å^3. Data analysis was performed by analyzing simulation results at a frequency of 5 ps. For each instance, the interaction energy of a DMS molecule with substrate was determined by calculating the change in potential energy of the system when that molecule is removed. Note that negative interaction energies (making up 3 out of ~15,000 sampled energies) were treated as outliers and thus ignored.

RESULTS AND DISCUSSION

Nanoparticle Morphology and Characterization. Standard PXRD, TEM, and DRS measurements were performed to verify that precipitation of CuI and AgI mixtures produced heterometallic nanoparticles. Spectra from these measurements can be found in the supporting information (ESI). PXRD analysis of **1** (Figure S1) confirmed the expected cubic diffraction pattern of γ-CuI (zinc blende structure). PXRD traces for **2** and **3** show the same cubic pattern as that seen in **1**, but with increased lattice parameter (see Figure S1, ESI). No additional PXRD peaks attributable to pure CuI or AgI were observed in the mixed nanoparticle samples **2** and **3**. Thus, the analogous PXRD patterns for the three samples were consistent with homogenous zinc blende phases. TEM images of **1**-**3** (Figure S2) confirm the presence of spherical nanoparticles that are relatively monodispersed. Average diameters for **1** of 18.3 ± 2.6 nm, **2** of 20.2 ± 1.4 nm, and **3** of 45 ± 5.7 nm were determined by ImageJ particle analysis of multiple micrograph images.[57] While solid samples of **1** are off-white in color, **2** and **3** are distinctly more yellow. Diffuse reflectance measurements (Figure S3) for **1**-**3** reveal strong absorption bands in the UV and visible range for all samples. It is clear from the spectra that **2** and **3** have distinctly broader bands compared to **1** and extend further into visible range, in agreement with observed colors. The calculated band gap energies of **1**-**3** using the optical absorption edge are 2.93 eV, 2.79 eV, and 2.62 eV, respectively. It becomes apparent that as the concentration of Ag is increased, the band gap energy is decreased. These band gap energies are similar to previously reported bulk and nano-γ-CuI/AgI systems with band gaps ranging between 2.92 eV and 3.1 eV.[58–63] Because of this we believe that these nanoparticles retain the known semi-conductive properties of homometallic CuI and AgI films, an important property with respect to developing optoelectronic devices.[64]

Vapochromic Behavior. To explore the vapochromic behavior of the metal iodides we have measured the luminescence of solid samples before (**1**-**3**) and after (**1′-3′**) exposure to DMS vapor, now designated with a prime. Unexposed nanoparticles **1** and **2** show pink emission under UV light, Figure 2. This pink emission is noticeably reduced with increasing Ag content whereby **3** is completely *non-emissive*. Presumably this emissive behavior is due to a halide-metal charge transfer (XMCT) between the I 6*s* and Cu 3*d* atomic orbitals which has been reported in CuI films.[16]

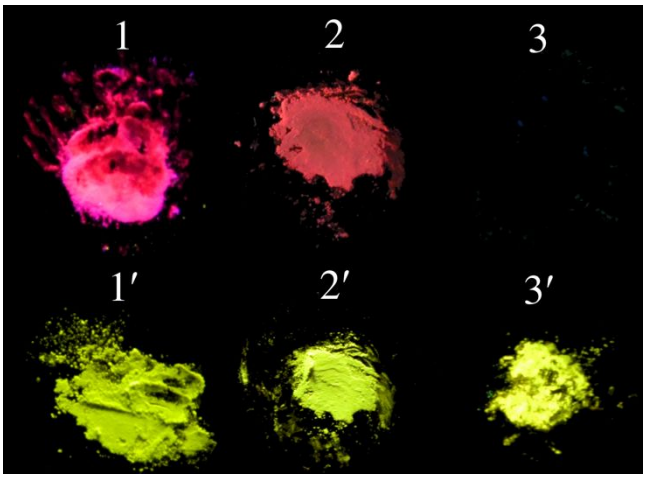

Figure 2. Images under UV light before (**1**-**3**) and after (**1′-3′**) exposure to DMS vapor.

Upon exposure to DMS vapor, vapochromic behavior is observed for **1′-3′** by the appearance of bright green emission. Solid state luminescence measurements of exposed **1′-3′** (Figure S9) reveal identical emission bands with a peak at 550 nm.

Thermogravimetric analysis (TGA) for **1′-3′** shows thermal removal of the DMS in the range of 50-80 °C (Figure S4). Sample **1′** showed a DMS content of 18.2% by mass, while Ag-containing **2′** and **3′** showed only 5.5% and 8.0% DMS respectively. Vacuum exposure (100 μm Hg) over several days removed all the DMS from **1′-3′** as confirmed by both PXRD and TGA (Figures S4-S7). Nevertheless, exposed nanoparticles show moderate stability at STP, showing loss of green emission over the course of several hours (Figure S8).

In order to further analyze the vapochromic behavior, the emission spectra were compared to the previously reported copper-iodide cluster complexes $[CuI]_n[DMS]_3$.[65–67] In reactions of CuI with neat DMS both ligand-rich $[CuI]_2[DMS]_3$ and ligand-poor $[CuI]_4[DMS]_3$ complexes have been reported. The ligand-rich $[CuI]_2[DMS]_3$ complex is non-emissive under UV light and readily decomposes to the ligand-poor complex $[CuI]_4[DMS]_3$ (Figure S10 and S11).[66] Under UV light (350 nm) irradiation $[CuI]_4[DMS]_3$ is highly emissive, with emission at 549 nm, which value is nearly identical to that of **1′-3′**. This agreement in emission energies points to the formation of the open-flower-basket ligand-poor complex $[CuI]_4[DMS]_3$ as the emissive species of **1′-3′**. Oddly, identical emission energy values are found irrespective of the Cu/Ag metal ratio, implying that Ag(I) ions are not participating in final coordination of the DMS. This behavior is highlighted by reports on analogous complexes of Cu(I)/Ag(I) wherein drastic differences in emission energy are observed when coordination occurs at Cu(I) sites versus Ag(I) sites.[68–70] For example in the cubane complexes $Cu_4I_4(PPh_3)_4$ and $Ag_4I_4(PPh_3)_4$ at 120 K the maximum emission energy is 570 nm and 465 nm, respectively.[65,68,69,71–73] If DMS coordination to Ag(I) were occurring in **1′-3′** we would reasonably expect to observe differences in energy between emission bands. Since this is not the case, we are led to believe that Ag(I) does not participate in formation of the final emissive product. This leaves only the Cu(I) as a final coordination site, ultimately forming $[CuI]_4[DMS]_3$ clusters at the nanoparticle surface.

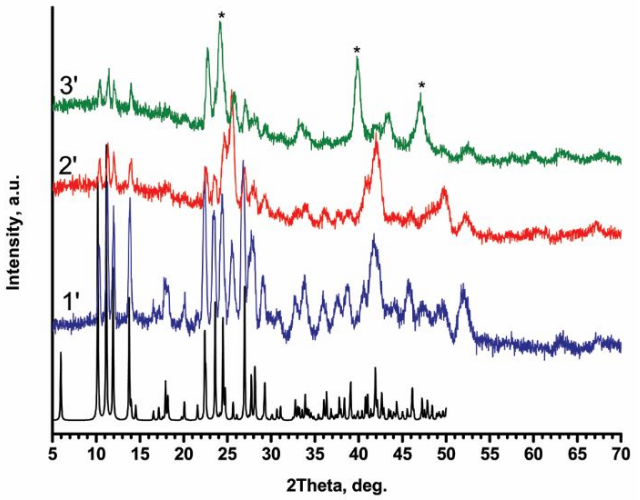

Figure 3. PXRD spectra of **1′-3′** (samples after exposure to DMS vapor). Calculated PXRD of $[CuI]_4[DMS]_3$ provided in black.[65] γ-CuI/AgI peaks noted by *.

We performed PXRD on the post-exposure samples **1′-3′** (Figure 3). In all cases the major phase observed is $[CuI]_4[DMS]_3$, matching the calculated pattern. Nevertheless, the zinc blende γ-CuI/AgI phase seen in the unexposed samples **1-3** is still evident in **1′-3′** (starred peaks). This finding is unsurprising given that the formation of luminescent product resulting from DMS vapor exposure is necessarily a surface phenomenon, leaving the particle cores unchanged. The match between that **1′-3′** PXRD the calculated $[CuI]_4[DMS]_3$ pattern strongly supports the assertion that the final emissive DMS adduct is free of Ag(I).

Molecular Dynamics. The mechanism by which the hetero-metallic nanoparticles react to selectively form $[CuI]_4[DMS]_3$ is not known. Thus, in order to understand the structural and kinetic features of these nanoparticles, Molecular Dynamics calculations were performed. To accomplish this, DMS monolayers were modeled for (111) cation-terminated surfaces of copper iodide crystals doped with variable amounts of silver. Simulations revealed that doping with silver results in stronger binding of DMS molecules to (111) surface sites (See Figure 4). The majority of DMS molecules (i.e. 77%) are bound to metal centers with coordination numbers of 2 or 3 (determined using a cutoff sulfur-metal distance of 4.2 Å for both copper and silver ions). For these molecules, the average binding energy for the silver-doped substrate is 1.2 kJ/mol greater than that of pure copper iodide substrate. We suggest that this effect would lead to enhanced adsorption of DMS vapor onto silver-doped substrates. DMS molecules that embed themselves into the substrate structure will, as a result, produce a metal coordination number of 5. In these cases, the average binding energy difference is even greater for silver-doped substrates, in the range of 4 to 12 kJ/mol. We argue that this enhanced stability of high-coordination states observed for silver-doped substrate could catalyze cluster formation, thus providing one possible explanation for the kinetics results observed in this work. Surprisingly, the strongest DMS interactions were observed for 25% AgI substrate, not 50% AgI. These strongest interactions in 25% AgI are found to be heterometallic in nature (as is discussed later). Additionally, the average metal coordination number for a DMS molecule was 2.14, 2.22, and 2.23, for pure CuI, 25% AgI, and 50% AgI, respectively. Average coordination numbers are thus greater when silver dopant is present, further demonstrating that the destabilization effect of silver dopant within the lattice causes a stronger interaction between the substrate and the DMS vapor.

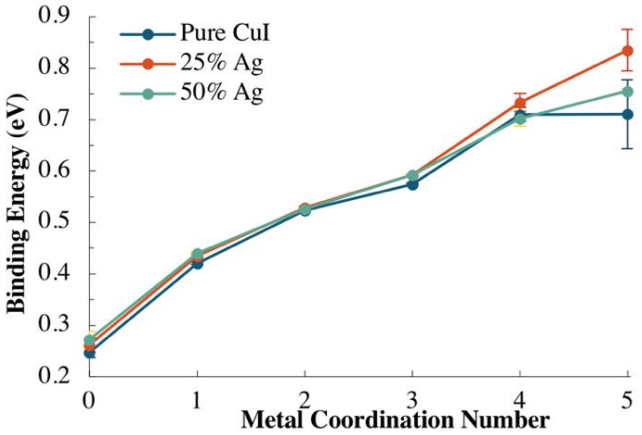

Figure 4. Binding energy vs. metal coordination number (CN). Increasing CN results in stronger interactions with substrate. Standard errors of the mean are shown. (Note: the five-coordinated state is relatively rare, making up only 0.13% of sampled states.)

Several instances of the embedding of DMS molecules into surface defect sites have been detected for all three systems (i.e. pure copper, 25% Ag, and 50% Ag). This happened multiple times for each system, with a total of about twenty instances being detected (note: detection of embedded states was here performed by scanning results for a metal coordination number of 5 or an iodide coordination number of 7, using a cutoff sulfur-iodide

distance of 4.7 Å). The most noteworthy incident of embedding occurred for 25% Ag (see Figure 5). In this case, a DMS molecule was found to embed into the surface step over a relatively long timeframe of about 60 ps, exhibiting a relatively high average binding energy of 0.92 eV, an average copper coordination number of 2.2, an average silver coordination number of 1.7, and an average iodide coordination number of 6.9. This interaction thus demonstrates how heterometallic character leads to strong substrate-vapor interactions. To assess the reversibility of monolayer formation, a DMS monolayer on pure CuI (taken from these simulation results) was simulated for 5 ns under vacuum conditions at a temperature of either 25 °C (k_BT = 0.026 eV) or 120 °C (k_BT = 0.034 eV). At 25 °C, only 5% of the DMS molecules evaporated. At 120 °C, 81% of the DMS molecules evaporated. This large difference suggests that increasing the temperature is essential to fully baking off the DMS monolayer, in agreement with our experimental findings.

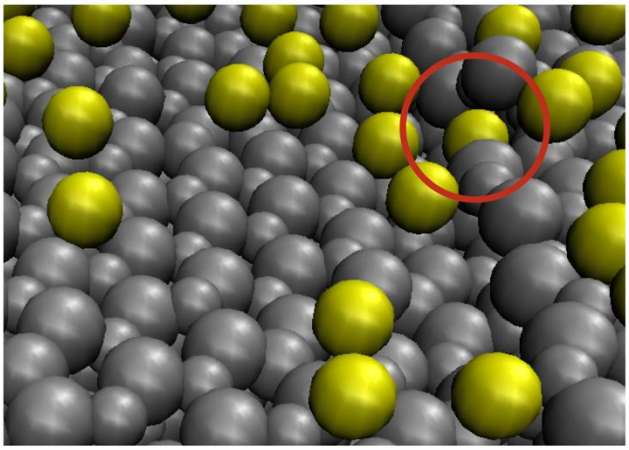

Figure 5. DMS molecule embedded into surface step site (circled in red). For simplicity, only the sulfur atoms of the DMS molecules are shown and all substrate atoms are given silver color. Along the surface step, substrate atoms can be seen to be displaced by a sulfur atom. We suggest that this embedded state is an intermediary in the formation of the product complex. (Image made with VMD.[55])

Overall, simulations show that heterometallic character of the substrate strengthens the binding of DMS molecules to the surface and results in strong embedded-state interactions. To our knowledge, this is the first report of such behavior. Further investigation (with much greater data sampling and more doping levels considered) would be necessary to determine quantitative relationships between the amount of silver doping and binding characteristics.

Kinetic Treatment. Experimental kinetic measurements were performed to corroborate the unexpected molecular dynamic simulation results. We first consider the reaction of metal halide nanoparticles with nucleophilic vapors as a three-step mechanism: (1) rapid adsorption of nucleophilic vapors to the surface dictated by weak electrostatic interactions, (2) embedding of the DMS molecule into the surface as an intermediate, and (3) rearrangement of the surface to form the final $[CuI]_4[DMS]_3$ product.

(1) $A + B \underset{k_{-1}}{\overset{k_1}{\rightleftarrows}} [A\cdots B]$ Rapid (ps) adsorption

(2) $[A\cdots B] \underset{k_{-2}}{\overset{k_2}{\rightleftarrows}} [I]$ Fast (ns) embedding

(3) $I \xrightarrow{k_3} P$ Slow (s) rearrangement

It is possible to solve the associated rate law equations through rigorous mathematical treatment. However, controlling the experimental design allows for simplification of this complex mechanism. In our kinetics experiments we employed flooding conditions by using high concentrations and flow rates of DMS vapor in equation 1. Reactions were carried out at two different flow rates to confirm that flooding conditions had been met. In effect, *via* Le Châtelier's principle, the equilibrium is shifted towards the products, reducing the first step into a non-reversible reaction, with $k_1 >> k_{-1}$, whereby k_{-1} is negligible. In addition, Molecular Dynamics calculations show that the electrostatic interactions are established rapidly (on the order of picoseconds) in comparison to the embedding of DMS vapor. Thus, as $k_1 >> (k_2 + k_{-2})$, and in combination of flooding with DMS the formation of a DMS monolayer [A···B], can be considered as being instantaneous at high concentration. This is important because it becomes possible to consider the formation of the embedded DMS as the initial step in the reaction, reducing the three-step mechanism to a two-step mechanism.

(4) $[A\cdots B] \underset{k_{-2}}{\overset{k_2}{\rightleftarrows}} [I]$ Fast (ns)

(5) $I \xrightarrow{k_3} P$ Slow (s)

While the method of analysis for a non-steady state consecutive reaction, first step reversible, has been determined, solving the rate constants requires complex integration.[74] Since the second step is dependent only on [A···B], whose initial concentration is maintained by continuous flow of DMS vapor, we can treat the second step *via* $k_2 << k_{-2}$, as a nonreversible reaction. Finally, the exposed nanoparticles do not rapidly lose DMS, showing open-air stability over several hours (Figure S8), indicating that the overall reverse reaction is much slower, and thus further supporting our treatment of the final rearrangement step as nonreversible. Eliminating the rapid adsorption step and treating the embedding of DMS vapor into the surface and the rearrangement as a nonreversible step, we can rewrite the overall mechanistic expression as a series of consecutive first order reactions (6) for which analysis is much less complex.[75,76]

(6) $[A\cdots B] \overset{k_2}{\rightarrow} I \overset{k_3}{\rightarrow} P$

Here, the equation for the formation of the observable product [P] over time is dictated by equation (7) below, as solved elsewhere.[75]

(7) $[P]_t = [A + B]_0\left\{1 - \frac{1}{k_3 - k_2}\left\{k_2 e^{(-k_2 t)} - k_1 e^{(-k_3 t)}\right\}\right\}$

To determine the rate constants, we have varied the k_2 and k_3 values to produce a best fit line with a minimum RMS value compared to the experimental data. It is important to note that two solutions to the above equation exist in which the values of k_2 and k_3 are interchanged. The solutions correspond to either rapid formation of a weakly emitting intermediate or slow formation of a strongly emitting intermediate.[75] Since emission in $Cu_4I_4(DMS)_3$ is dependent on close Cu-Cu distances of less than the sum of the van der Waals radii, it is not possible for the intermediate to be emissive.[65] Thus, we can rule out the slow formation of a strongly emissive intermediate, leaving only the possibility of rapid formation of a weakly emitting intermediate. This assertion is

further supported by our molecular dynamic calculations which show that DMS embeds into the surface rapidly (order of nanoseconds). Thus, we believe that the third step is the rate-determining step, and thus $k_2 >> k_3$.

Kinetic Studies. We believe that the vapochromic response of d^{10} metal-halide nanoparticles occurs *via* a reduced three-step process: (1) adsorption of the nucleophile on the surface, (2) embedding of the DMS molecules into the surface of the nanoparticles, and (3) formation of the final $[CuI]_4[DMS]_3$ product. Kinetics evidence supports this mechanism. Thus, during initial DMS exposure we measured nanoparticle emission as a function of time until the nanoparticles were saturated and showed no further emission change. We present our results for **1-3** in Figure 6 and Table 1. The time-dependent emission spectra indicate that the pure metal halide **1** reacts more *slowly* than the mixed metal halide nanoparticles **2** and **3** as evident by the order of 1st half-lives for **3** << **2** < **1** (9.85 s, 74.2 s and 97.7 s, respectively). Calculation of rate constants reveals that in all cases, the rearrangement of the

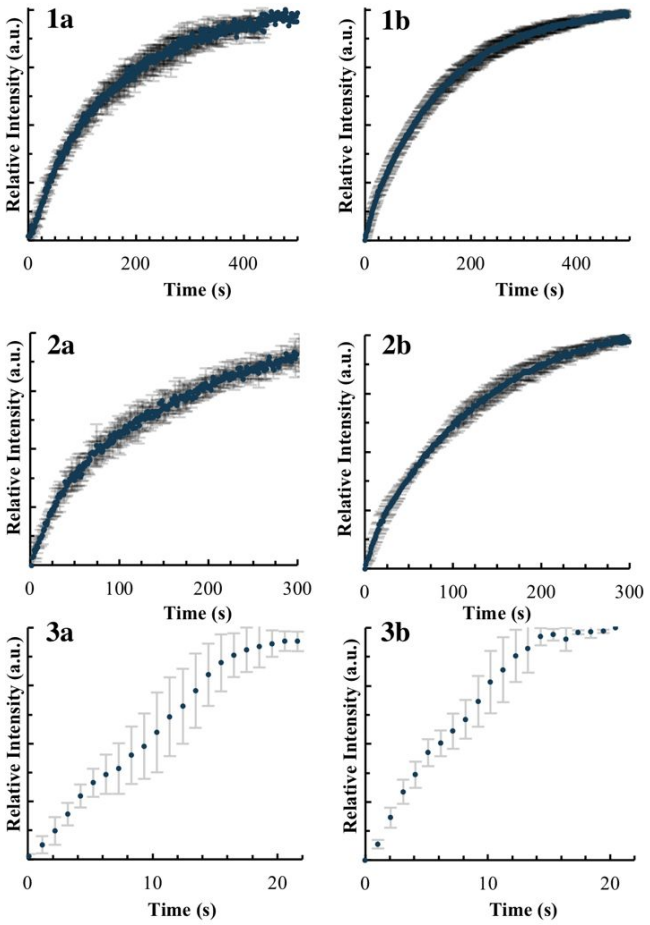

Figure 6. Kinetics measurements of **1-3** during exposure to DMS vapor. Graphs show emission intensity versus exposure time at (**1a-3a**) 43.3 μmol hr^{-1} and (**1b-3b**) 86.7 μmol hr^{-1}. Each graph is the average of three trials, error bars represent one standard deviation.

surface DMS to form the $[CuI]_4[DMS]_3$ phase is the rate-determining step, by an order of 10^4-10^5. The magnitude of k_2 differs very little amongst **1**, **2**, and **3**. Instead, k_3 acts as the metal-dependent value, increasing with higher concentrations of Ag(I). This increase leads to the significantly faster reaction rate of **3**, for which the reaction is complete within 30 s. It is important to reiterate at this point that the final emissive product $[CuI]_4[DMS]_3$ is *identical* for **1′-3′**, as is evident from the PXRD and luminescence spectra, despite the differences in substrate composition.

Table 1. Summary of kinetics results for **1-3** upon exposure to DMS vapor. Results shown for DMS flow rates of 43.3 μmol hr^{-1} and 86.7 μmol hr^{-1}.

Substrate	Flow Rate	Half-life	k_2	k_3
1	43.3 μmol hr^{-1}	97.7 s	$>10^2$	7.32×10^{-3}
	86.7 μmol hr^{-1}	96.4 s	$>10^2$	7.38×10^{-3}
2	43.3 μmol hr^{-1}	74.2 s	$>10^2$	8.88×10^{-3}
	86.7 μmol hr^{-1}	72.4 s	$>10^2$	8.89×10^{-3}
3	43.3 μmol hr^{-1}	9.85 s	$>10^2$	8.09×10^{-2}
	86.7 μmol hr^{-1}	6.14 s	$>10^2$	8.19×10^{-2}

To probe the effect of Ag(I) substitution on our kinetic mechanism we have calculated the activation energy for the reaction of **1-3** with DMS. Since rearrangement of the surface to form the final product is the slow and represents the overall rate determining step, we need only focus on the final reaction rate involving k_3 of **1-3,** $k_3^{\mathbf{1}}$, $k_3^{\mathbf{2}}$, $k_3^{\mathbf{3}}$, respectively. Utilizing the Arrhenius equation, we can relate each rate constant to the system's activation energy for each case as shown below:

(8) Sample **1**: $k_3^{\mathbf{1}} = Ae^{\frac{-E_{a1}}{RT}}$

(9) Sample **2**: $k_3^{\mathbf{2}} = Ae^{\frac{-E_{a2}}{RT}}$

(10) Sample **3**: $k_3^{\mathbf{3}} = Ae^{\frac{-E_{a3}}{RT}}$

where R = 8.314 $^{J}/_{mol\text{-}K}$, T = 298 K, A is the unknown frequency factor, and the values E_{a1}, E_{a2}, and E_{a3} are the activation energies of **1**, **2**, and **3**, respectively. Since the reactions are carried out under identical experimental conditions, we assume that the frequency factor is the same for each reaction. Removal of the unknown frequency variable is achieved by dividing equations 8-10 pairwise, and can be rearranged and simplified to the forms:

(11) $$\ln\left(\frac{k_3^{\mathbf{1}}}{k_3^{\mathbf{2}}}\right) = (-E_{a1} + E_{a2})\left(\frac{1}{RT}\right)$$

(12) $$\ln\left(\frac{k_3^{\mathbf{1}}}{k_3^{\mathbf{3}}}\right) = (-E_{a1} + E_{a3})\left(\frac{1}{RT}\right)$$

(13) $$\ln\left(\frac{k_3^{\mathbf{2}}}{k_3^{\mathbf{3}}}\right) = (-E_{a2} + E_{a3})\left(\frac{1}{RT}\right)$$

A direct algebraic solution of the above equations for the activation energies using the addition/subtraction method does not exist. Thus, we are required to make an assumption as to the *relative* activation energies between reactions. Utilizing $k \propto 1/E_a$ we assume that E_{a1} is proportionate to E_{a3} by the ratio $k_3^{\mathbf{1}}/k_3^{\mathbf{3}}$. This assumption provides the expression:

(14) $$\frac{k_3^{\mathbf{1}}}{k_3^{\mathbf{3}}}E_{a1} = E_{a3}$$

where the combination of equations 11-14 permits the solution of the activation energies (Table 2). It is clear from the results that incorporation of Ag(I) ions into the nanoparticle drastically affects

the activation energy of the overall reaction. In this study a 25% and 50% Ag(I) content resulted in a reduction of the activation energy by 7% and 91%, respectively, demonstrating DMS-sensing enhancement in heterometallic vs homometallic materials.

Table 2. Calculated activation energies for **1-3** for reaction with DMS vapor.

Substrate	Activation Energy
1	6550 $^{J}/_{mol\text{-}K}$
2	6080 $^{J}/_{mol\text{-}K}$
3	591 $^{J}/_{mol\text{-}K}$

CONCLUSION

In summary, we have probed the vapochromic behavior of homo- and heterometallic Cu/AgI nanoparticles towards DMS vapor. We have discovered that introduction of Ag(I) into the synthesis of CuI nanoparticles does not change the overall zinc blende structure of the nanoparticle, nor the final luminescent species upon exposure to DMS vapor. Molecular Dynamics calculations indicate that heterometallic character strengthens the binding of DMS molecules to the surface and results in strong embedded-state interactions. Kinetic results for the vapochromic reactions between **1-3** and DMS vapor generally agree with those calculations, and we therefore suggest that the time-dependent measurements follow a three-step mechanism: (1) adsorption of DMS onto the surface, (2) embedding of the DMS into the surface of the nanoparticles, and (3) formation of the final $[CuI]_4[DMS]_3$ product. In DMS-flooded experiments, embedding of the DMS molecule into the surface forms the initial intermediate in the reaction. Kinetic analysis reveals that incorporation of Ag(I) ions into the nanoparticles greatly increases the reaction rate, with $Cu_{0.5}Ag_{0.5}I$ nanoparticle reaction half-life an order of magnitude less than that of CuI nanoparticles. The findings in this study suggest that mixed metal systems are able to perform more efficiently than single metal analogs *via* stronger interactions with incoming VOC vapors.

ASSOCIATED CONTENT

Supporting Information. Supporting Information contains powder X-ray diffraction, transmission electron microscopy, UV-vis diffuse reflectance, thermogravimetry, FTIR, and solid-state luminescence data of **1-3** and **1′-3′**. This material is available free of charge via the Internet at http://pubs.acs.org.

AUTHOR INFORMATION

Corresponding Authors

*aaron.d.nicholas@maine.edu, rdpike@wm.edu

Notes

The authors declare no competing financial interests.

Author Contributions

The manuscript was written through contributions of all authors. All authors have given approval to the final version of the manuscript.

Funding Sources

We acknowledge support from National Science Foundation (CHE-1413641 and CHE-0443345), the Welch Foundation (B-1542), and the College of William and Mary.

ACKNOWLEDGMENT

We thank the University of Maine Advanced Computing Group for their support and generous allocation of computing resources.

REFERENCES

(1) Pyykkö, P. Strong Closed-Shell Interactions in Inorganic Chemistry. *Chem. Rev.* **1997**, *97* (3), 597–636. https://doi.org/10.1021/cr940396v.

(2) Pyykkö, P.; Li, J.; Runeberg, N. Predicted Ligand Dependence of the Au(I)…Au(I) Attraction in $(XAuPH_3)_2$. *Chem. Phys. Lett.* **1994**, *218* (1–2), 133–138. https://doi.org/10.1016/0009-2614(93)E1447-O.

(3) Liau, R.-Y.; Schier, A.; Schmidbaur, H. Oligomerization of Digoldacetylide Complexes through Angular Head-to-Tail Aurophilic Bonding. *Organometallics* **2003**, *22* (16), 3199–3204. https://doi.org/10.1021/om030164z.

(4) Burini, A.; Galassi, R.; Pietroni, B. R.; Burini, A.; Fackler Jr., J. P.; Galassi, R.; Staples, R. J. The First Sandwich Silver Cluster of a Trinuclear Cyclic Gold(I) Complex. *Chem. Commun.* **1998**, No. 1, 95–96. https://doi.org/10.1039/a706795j.

(5) Burini, A.; Mohamed, A. A.; Fackler, J. P. Cyclic Trinuclear Gold(I) Compounds: Synthesis, Structures and Supramolecular Acid-Base π-Stacks. *Comments Inorg. Chem.* **2003**, *24* (5–6), 253–280. https://doi.org/10.1080/02603590390464225.

(6) Yang, G.; Raptis, R. Supramolecular Assembly of Trimeric Gold(I) Pyrazolates through Aurophilic Attractions. *Inorg. Chem.* **2003**, *42*, 261–263. https://doi.org/10.1021/ic026051+.

(7) White-Morris, R. L.; Olmstead, M. M.; Jiang, F.; Balch, A. L. New Insights into the Effects of Self-Association of the Cation $[Au\{C(NHMe)_2\}_2]^+$ on Its Solid State Structure and Luminescence. *Inorg. Chem.* **2002**, *41* (9), 2313–2315. https://doi.org/10.1021/ic020030y.

(8) Leznoff, D. B.; Xue, B.-Y.; Batchelor, R. J.; Einstein, F. W. B.; Patrick, B. O. Gold−Gold Interactions as Crystal Engineering Design Elements in Heterobimetallic Coordination Polymers. *Inorg. Chem.* **2001**, *40* (23), 6026–6034. https://doi.org/10.1021/ic010756e.

(9) Markert, J. T.; Blom, N.; Roper, G.; Perregaux, A. D.; Nagasundaram, N.; Corson, M. R.; Ludi, A.; Nagle, J. K.; Patterson, H. H. Luminescence of Cesium Dicyanoaurate(I). Evidence for Extended Au(I)-Au(I) Interactions in Two Dimensions. *Chem. Phys. Lett.* **1985**, *118* (3), 258–262. https://doi.org/10.1016/0009-2614(85)85311-2.

(10) Scherbaum, F.; Grohmann, A.; Müller, G.; Schmidbaur, H. Synthesis, Structure, and Bonding of the Cation $[\{(C_6H_5)_3PAu\}_5C]^+$. *Angew. Chemie Int. Ed. English* **1989**, *28* (4), 463–465. https://doi.org/10.1002/anie.198904631.

(11) Schmidbaur, H. The Fascinating Implications of New Results in Gold Chemistry. *Gold Bull.* **1990**, *23* (1), 11–21. https://doi.org/10.1007/BF03214710.

(12) Schmidbaur, H. Ludwig Mond Lecture. High-Carat Gold Compounds. *Chem. Soc. Rev.* **1995**, *24* (6), 391. https://doi.org/10.1039/cs9952400391.

(13) Schmidbaur, H.; Hamel, A.; Mitzel, N. W.; Schier, A.; Nogai, S. Cluster Self-Assembly of Di[Gold(I)]Halonium Cations. *Proc. Natl. Acad. Sci.* **2002**, *99* (8), 4916–4921. https://doi.org/10.1073/pnas.062643599.

(14) Hettiarachchi, S. R.; Rawashdeh-Omary, M. A.; Kanan, S. M.; Omary, M. A.; Patterson, H. H.; Tripp, C. P. Spectroscopic Studies of "Exciplex Tuning" for Dicyanoaurate(I) Ions Doped in Potassium Chloride Crystals. *J. Phys. Chem. B* **2002**, *106* (39), 10058–10064. https://doi.org/10.1021/jp0209594.

(15) Omary, M. A.; Patterson, H. H. Luminescent Homoatomic Exciplexes in Dicyanoargentate(I) Ions Doped in Alkali Halide Crystals. 1. "Exciplex Tuning" by Site-Selective Excitation. *J. Am. Chem. Soc.* **1998**, *120* (31), 7696–7705. https://doi.org/10.1021/ja980256t.

(16) Killarney, J. P.; McKinnon, M.; Murphy, C.; Henline, K. M.;

Wang, C.; Pike, R. D.; Patterson, H. H. Amine- and Sulfide-Sensing Copper(I) Iodide Films. *Inorg. Chem. Commun.* **2014**, *40*, 18–21. https://doi.org/10.1016/j.inoche.2013.11.022.

(17) Miller, K. M.; McCullough, S. M.; Lepekhina, E. A.; Thibau, I. J.; Pike, R. D.; Li, X.; Killarney, J. P.; Patterson, H. H. Copper(I) Thiocyanate-Amine Networks: Synthesis, Structure, and Luminescence Behavior. *Inorg. Chem.* **2011**, *50* (15), 7239–7249. https://doi.org/10.1021/ic200821f.

(18) Safko, J. P.; Kuperstock, J. E.; McCullough, S. M.; Noviello, A. M.; Li, X.; Killarney, J. P.; Murphy, C.; Patterson, H. H.; Bayse, C. A.; Pike, R. D. Network Formation and Photoluminescence in Copper(I) Halide Complexes with Substituted Piperazine Ligands. *Dalt. Trans.* **2012**, *41* (38), 11663. https://doi.org/10.1039/c2dt31241g.

(19) Benito, Q.; Le Goff, X. F.; Nocton, G.; Fargues, A.; Garcia, A.; Berhault, A.; Kahlal, S.; Saillard, J.-Y.; Martineau, C.; Trébosc, J.; et al. Geometry Flexibility of Copper Iodide Clusters: Variability in Luminescence Thermochromism. *Inorg. Chem.* **2015**, *54*, 4483–4494. https://doi.org/10.1021/acs.inorgchem.5b00321.

(20) Elder, R.; Elder, K. Method for the Treatment of Retroviral Diseases Such as Acquired Immune Deficiency Syndrome Utilizing (Pseudo)Halogen Complexes of Gold(I). US5603963 A, 1997.

(21) Mansour, M. A.; Connick, W. B.; Lachicotte, R. J.; Gysling, H. J.; Eisenberg, R. Linear Chain Au(I) Dimer Compounds as Environmental Sensors: A Luminescent Switch for the Detection of Volatile Organic Compounds. *J. Am. Chem. Soc.* **1998**, *120* (6), 1329–1330. https://doi.org/10.1021/ja973216i.

(22) Varju, B. R.; Ovens, J. S.; Leznoff, D. B. Mixed Cu(I)/Au(I) Coordination Polymers as Reversible Turn-On Vapoluminescent Sensors for Volatile Thioethers. *Chem. Commun.* **2017**, *53* (48), 6500–6503. https://doi.org/10.1039/C7CC03428H.

(23) Daws, C. A.; Exstrom, C. L.; Sowa, J. R.; Mann, K. R. "Vapochromic" Compounds as Environmental Sensors. 2. Synthesis and Near-Infrared and Infrared Spectroscopy Studies of $[Pt(Arylisocyanide)_4][Pt(CN)_4]$ upon Exposure to Volatile Organic Compound Vapors. *Chem. Mater.* **1997**, *9* (1), 363–368. https://doi.org/10.1021/cm960397z.

(24) Dong, Y.; Lam, J. W. Y.; Li, Z.; Qin, A.; Tong, H.; Dong, Y.; Feng, X.; Tang, B. Z. Vapochromism of Hexaphenylsilole. *J. Inorg. Organomet. Polym. Mater.* **2005**, *15* (2), 287–291. https://doi.org/10.1007/s10904-005-5546-0.

(25) Fernández, E. J.; López-de-Luzuriaga, J. M.; Monge, M.; Olmos, M. E.; Pérez, J.; Laguna, A.; Mohamed, A. A.; Fackler, J. P. $\{Tl[Au(C_6Cl_5)_2]\}_n$: A Vapochromic Complex. *J. Am. Chem. Soc.* **2003**, *125* (8), 2022–2023. https://doi.org/10.1021/ja028734u.

(26) Fernández, E. J.; López-de-Luzuriaga, J. M.; Monge, M.; Montiel, M.; Olmos, M. E.; Pérez, J.; Laguna, A.; Mendizabal, F.; Mohamed, A. A.; Fackler, J. P. A Detailed Study of the Vapochromic Behavior of $\{Tl[Au(C_6Cl_5)_2]\}_n$. *Inorg. Chem.* **2004**, *43* (12), 3573–3581. https://doi.org/10.1021/ic0499446.

(27) Grate, J. W.; Moore, L. K.; Janzen, D. E.; Veltkamp, D. J.; Kaganove, S.; Drew, S. M.; Mann, K. R. Steplike Response Behavior of a New Vapochromic Platinum Complex Observed with Simultaneous Acoustic Wave Sensor and Optical Reflectance Measurements. *Chem. Mater.* **2002**, *14* (3), 1058–1066. https://doi.org/10.1021/cm0104506.

(28) Ni, J.; Wang, Y.-G.; Wang, J.-Y.; Zhao, Y.-Q.; Pan, Y.-Z.; Wang, H.-H.; Zhang, X.; Zhang, J.-J.; Chen, Z.-N. A New Sensor for Detection of CH_3CN and $ClCH_2CN$ Vapors Based on Vapoluminescent Platinum(II) Complex. *Dalt. Trans.* **2013**, *42* (36), 13092. https://doi.org/10.1039/c3dt51397a.

(29) Grove, L. J.; Oliver, A. G.; Krause, J. A.; Connick, W. B. Structure of a Crystalline Vapochromic Platinum(II) Salt. *Inorg. Chem.* **2008**, *47* (5), 1408–1410. https://doi.org/10.1021/ic701523e.

(30) Lee, C.-S.; Zhuang, R. R.; Sabiah, S.; Wang, J.-C.; Hwang, W.-S.; Lin, I. J. B. Size-Selective Vapochromic Platinum(II) Complex with a Sterically Demanding Pincer-Type N-Heterocyclic Carbene Ligand. *Organometallics* **2011**, *30* (14), 3897–3900. https://doi.org/10.1021/om200253f.

(31) Kishi, S.; Kato, M. Vapochromism and Crystal Structures of Luminescent Dicyano(2,2′-Bipyridine)Platinum(II). *Mol. Cryst. Liq. Cryst.* **2002**, *379* (1), 303–308. https://doi.org/10.1080/713738608.

(32) Lefebvre, J.; Batchelor, R. J.; Leznoff, D. B. $Cu[Au(CN)_2]_2(DMSO)_2$: Golden Polymorphs That Exhibit Vapochromic Behavior. *J. Am. Chem. Soc.* **2004**, *126* (49), 16117–16125. https://doi.org/10.1021/ja049069n.

(33) Matsushima, R.; Nishimura, N.; Goto, K.; Kohno, Y. Vapochromism of Ionic Dyes in Thin Films of Sugar Gels. *Bull. Chem. Soc. Jpn.* **2003**, *76* (6), 1279–1283. https://doi.org/10.1246/bcsj.76.1279.

(34) Buss, C. E.; Anderson, C. E.; Pomije, M. K.; Lutz, C. M.; Britton, D.; Mann, K. R. Structural Investigations of Vapochromic Behavior. X-Ray Single-Crystal and Powder Diffraction Studies of $[Pt(CN\text{-}Iso\text{-}C_3H_7)_4][M(CN)_4]$ for M = Pt or Pd. *J. Am. Chem. Soc.* **1998**, *120* (31), 7783–7790. https://doi.org/10.1021/ja981218c.

(35) Exstrom, C. L.; Sowa, J. R. J.; Daws, C. A.; Janzen, D.; Mann, K. R.; Moore, G. A.; Stewart, F. F. Inclusion of Organic Vapors by Crystalline, Solvatochromic $[Pt(Arylisonitrile)_4][Pd(CN)_4]$ Compounds. "Vapochromic" Environmental Sensors. *Chem. Mater.* **1995**, *7* (1), 15–17. https://doi.org/10.1021/cm00049a005.

(36) Wadas, T. J.; Wang, Q.-M.; Kim, Y.; Flaschenreim, C.; Blanton, T. N.; Eisenberg, R. Vapochromism and Its Structural Basis in a Luminescent Pt(II) Terpyridine−Nicotinamide Complex. *J. Am. Chem. Soc.* **2004**, *126* (51), 16841–16849. https://doi.org/10.1021/ja047955s.

(37) Yamada, K.; Yagishita, S.; Tanaka, H.; Tohyama, K.; Adachi, K.; Kaizaki, S.; Kumagai, H.; Inoue, K.; Kitaura, R.; Chang, H.-C.; et al. Metal-Complex Assemblies Constructed from the Flexible Hinge-Like Ligand H_2bhnq: Structural Versatility and Dynamic Behavior in the Solid State. *Chem. - A Eur. J.* **2004**, *10* (11), 2647–2660. https://doi.org/10.1002/chem.200305640.

(38) Exstrom, C. L.; Pomije, M. K.; Mann, K. R. Infrared Spectroscopy Studies of Platinum Salts Containing Tetracyanoplatinate(II). Evidence for Strong Hydrogen-Bonding Interactions in "Vapochromic" Environmental Sensor Materials. *Chem. Mater.* **1998**, *10* (3), 942–945. https://doi.org/10.1021/cm970788t.

(39) Balch, A. L.; Olmstead, M. M.; Vickery, J. C. Gold(I) Compounds without Significant Aurophilic Intermolecular Interactions: Synthesis, Structure, and Electronic Properties of $Ph_3PAuC(O)NHMe$ and $Au_3(PhCH_2NCOMe)_3$: Comparative Monomeric and Trimeric Analogues of the Solvoluminescent Trimer, Au_3. *Inorg. Chem.* **1999**, *38* (15), 3494–3499. https://doi.org/10.1021/ic990080b.

(40) Fung, E. Y.; Olmstead, M. M.; Vickery, J. C.; Balch, A. L. Glowing Gold Rings: Solvoluminescence from Planar Trigold(I) Complexes. *Coord. Chem. Rev.* **1998**, *171*, 151–159. https://doi.org/10.1016/S0010-8545(98)90025-X.

(41) Olmstead, M. M.; Jiang, F.; Attar, S.; Balch, A. L. Alteration of the Aurophilic Interactions in Trimeric Gold(I) Compounds through Charge Transfer. Behavior of Solvoluminescent $Au_3(MeNCOMe)_3$ in the Presence of Electron Acceptors. *J. Am. Chem. Soc.* **2001**, *123* (14), 3260–3267. https://doi.org/10.1021/ja0029533.

(42) White-Morris, R. L.; Olmstead, M. M.; Attar, S.; Balch, A. L. Intermolecular Interactions in Polymorphs of Trinuclear Gold(I) Complexes: Insight into the Solvoluminescence of $AuI_3(MeNCOMe)_3$. *Inorg. Chem.* **2005**, *44* (14), 5021–5029. https://doi.org/10.1021/ic050381n.

(43) Ovens, J. S.; Leznoff, D. B. Raman Detected Sensing of Volatile Organic Compounds by Vapochromic $Cu[AuX_2(CN)_2]_2$ (X = Cl, Br) Coordination Polymer Materials. *Chem. Mater.* **2015**, *27* (5), 1465–1478. https://doi.org/10.1021/cm502998w.

(44) Lefebvre, J.; Korčok, J. L.; Katz, M. J.; Leznoff, D. B. Vapochromic Behaviour of $M[Au(CN)_2]_2$-Based Coordination Polymers (M = Co, Ni). *Sensors* **2012**, *12* (12), 3669–3692. https://doi.org/10.3390/s120303669.

(45) Centre, C. C. D. Mercury 3.9. 2016.

(46) Welch, D. A.; Woehl, T. J.; Park, C.; Faller, R.; Evans, J. E.; Browning, N. D. Understanding the Role of Solvation Forces on the Preferential Attachment of Nanoparticles in Liquid. *ACS Nano* **2016**, *10* (1), 181–187. https://doi.org/10.1021/acsnano.5b06632.

(47) Bussi, G.; Donadio, D.; Parrinello, M. Canonical Sampling Through Velocity Rescaling. *J. Chem. Phys.* **2007**, *126* (1),

014101. https://doi.org/10.1063/1.2408420.
(48) Vashishta, P.; Rahman, A. Nature of Ionic Motions in AgI and CuI; United States, 1979.
(49) Bentenitis, N.; Cox, N. R.; Smith, P. E. A Kirkwood−Buff Derived Force Field for Thiols, Sulfides, and Disulfides. *J. Phys. Chem. B* **2009**, *113* (36), 12306–12315. https://doi.org/10.1021/jp904806f.
(50) Cornell, W. D.; Cieplak, P.; Bayly, C. I.; Gould, I. R.; Merz, K. M.; Ferguson, D. M.; Spellmeyer, D. C.; Fox, T.; Caldwell, J. W.; Kollman, P. A. A Second Generation Force Field for the Simulation of Proteins, Nucleic Acids, and Organic Molecules. *J. Am. Chem. Soc.* **1995**, *117* (19), 5179–5197. https://doi.org/10.1021/ja00124a002.
(51) Heinz, H.; Vaia, R. A.; Farmer, B. L.; Naik, R. R. Accurate Simulation of Surfaces and Interfaces of Face-Centered Cubic Metals Using 12−6 and 9−6 Lennard-Jones Potentials. *J. Phys. Chem. C* **2008**, *112* (44), 17281–17290. https://doi.org/10.1021/jp801931d.
(52) Gotlib, I. Y.; Ivanov-Schitz, A. K.; Murin, I. V.; Petrov, A. V.; Zakalyukin, R. M. Computer Simulation of Ionic Transport in Silver Iodide within Carbon Nanotubes. *Solid State Ionics* **2011**, *188* (1), 6–14. https://doi.org/10.1016/j.ssi.2010.11.020.
(53) Toxvaerd, S.; Dyre, J. C. Communication: Shifted Forces in Molecular Dynamics. *J. Chem. Phys.* **2011**, *134* (8), 081102. https://doi.org/10.1063/1.3558787.
(54) Fennell, C. J.; Gezelter, J. D. Is the Ewald Summation Still Necessary? Pairwise Alternatives to the Accepted Standard for Long-Range Electrostatics. *J. Chem. Phys.* **2006**, *124* (23), 234104. https://doi.org/10.1063/1.2206581.
(55) Humphrey, W.; Dalke, A.; Schulten, K. VMD: Visual Molecular Dynamics. *J. Mol. Graph.* **1996**, *14* (1), 33–38. https://doi.org/10.1016/0263-7855(96)00018-5.
(56) Kumar, P.; Starr, F. W.; Buldyrev, S. V.; Stanley, H. E. Effect of Water-Wall Interaction Potential on the Properties of Nanoconfined Water. *Phys. Rev. E* **2007**, *75* (1), 011202. https://doi.org/10.1103/PhysRevE.75.011202.
(57) Schneider, C. A.; Rasband, W. S.; Eliceiri, K. W. NIH Image to ImageJ: 25 Years of Image Analysis. *Nat. Methods* **2012**, *9* (7), 671–675. https://doi.org/10.1038/nmeth.2089.
(58) Amalina, M. N.; Rasheid, N. A.; Rusop, M. The Properties of Sprayed Nanostructured P-Type CuI Films for Dye-Sensitized Solar Cells Application. *J. Nanomater.* **2012**, 1–6. https://doi.org/10.1155/2012/637637.
(59) Lin, G.; Zhao, F.; Zhao, Y.; Zhang, D.; Yang, L.; Xue, X.; Wang, X.; Qu, C.; Li, Q.; Zhang, L. Luminescence Properties and Mechanisms of CuI Thin Films Fabricated by Vapor Iodization of Copper Films. *Materials (Basel).* **2016**, *9* (12), 990. https://doi.org/10.3390/ma9120990.
(60) Zhao, K.; Ngongang Ndjawa, G. O.; Jagadamma, L. K.; Labban, A. El; Hu, H.; Wang, Q.; Li, R.; Abdelsamie, M.; Beaujuge, P. M.; Amassian, A. Highly Efficient Organic Solar Cells Based on a Robust Room-Temperature Solution-Processed Copper Iodide Hole Transporter. *Nano Energy* **2015**, *16*, 458–469. https://doi.org/10.1016/j.nanoen.2015.07.018.
(61) Mochizuki, S.; Fujishiro, F. Structural, Electrical and Optical Studies on AgI–Anatase Composites. *J. Phys. Condens. Matter* **2003**, *15* (29), 5057–5072. https://doi.org/10.1088/0953-8984/15/29/317.
(62) Bharathi Mohan, D.; Sreejith, K.; Sunandana, C. S. Surface Plasmon–Exciton Transition in Ultra-Thin Silver and Silver Iodide Films. *Appl. Phys. B* **2007**, *89* (1), 59–63. https://doi.org/10.1007/s00340-007-2768-6.
(63) Mohan, D. B.; Reddy, V. S.; Sunandana, C. S. AgI Nanostructure Development in Sputter-Disordered and Al-Doped Ag Films Probed by XRD, SEM, Optical Absorption and Photoluminescence. *Appl. Phys. A* **2006**, *86* (1), 73–82. https://doi.org/10.1007/s00339-006-3727-5.
(64) Bouscher, S.; Panna, D.; Hayat, A. Semiconductor–Superconductor Optoelectronic Devices. *J. Opt.* **2017**, *19* (10), 103003. https://doi.org/10.1088/2040-8986/aa8888.
(65) Zhou, J.; Bian, G.-Q.; Dai, J.; Zhang, Y.; Zhu, Q.-Y.; Lu, W. Luminescent 2-D Double-Layered Polymer, $[(CuI)_4(CH_3SCH_3)_3]_\infty$, Containing Helical Chains Constructed by Flower-Basket-Shaped Cu_4I_4 Clusters. *Inorg. Chem.* **2006**, *45* (21), 8486–8488. https://doi.org/10.1021/ic060972t.
(66) Knorr, M.; Bonnot, A.; Lapprand, A.; Khatyr, A.; Strohmann, C.; Kubicki, M. M.; Rousselin, Y.; Harvey, P. D. Reactivity of CuI and CuBr toward Dialkyl Sulfides RSR: From Discrete Molecular $Cu_4I_4S_4$ and $Cu_8I_8S_6$ Clusters to Luminescent Copper(I) Coordination Polymers. *Inorg. Chem.* **2015**, *54* (8), 4076–4093. https://doi.org/10.1021/acs.inorgchem.5b00327.
(67) Maelger, H.; Olbrich, F.; Kopf, J.; Abeln, D.; Weiss, E. Synthese Und Struktur Der Basenaddukte von Kupfer(I)-Halogeniden Mit Dimethylsulfid Und Tetrahydrothiophen / Synthesis and Crystal Structure of Lewis Base Adducts of Copper(I)-Halides with Dimethylsulfide and Tetrahydrothiophene. *Zeitschrift für Naturforsch. B* **1992**, *47* (9), 1276–1280. https://doi.org/10.1515/znb-1992-0911.
(68) Perruchas, S.; Tard, C.; Le Goff, X. F.; Fargues, A.; Garcia, A.; Kahlal, S.; Saillard, J.-Y.; Gacoin, T.; Boilot, J.-P. Thermochromic Luminescence of Copper Iodide Clusters: The Case of Phosphine Ligands. *Inorg. Chem.* **2011**, *50*, 10682–10692. https://doi.org/10.1021/ic201128a.
(69) Henary, M.; Zink, J. I. Luminescence from the Chair and Cube Isomers of Tetrakis[(Triphenylphosphine)Iodosilver]. *Inorg. Chem.* **1991**, *30* (15), 3111–3112. https://doi.org/10.1021/ic00015a036.
(70) Shibata, S.; Tsuge, K.; Sasaki, Y.; Ishizaka, S.; Kitamura, N. Directional Energy Transfer in Mixed-Metallic Copper(I)-Silver(I) Coordination Polymers with Strong Luminescence. *Inorg. Chem.* **2015**, *54*, 9733–9739. https://doi.org/10.1021/acs.inorgchem.5b01224.
(71) De Angelis, F.; Fantacci, S.; Sgamellotti, A.; Cariati, E.; Ugo, R.; Ford, P. C. Electronic Transitions Involved in the Absorption Spectrum and Dual Luminescence of Tetranuclear Cubane $[Cu_4I_4(Pyridine)_4]$ Cluster: A Density Functional Theory/Time-Dependent Density Functional Theory Investigation. *Inorg. Chem.* **2006**, *45* (26), 10576–10584. https://doi.org/10.1021/ic061147f.
(72) Vitale, M.; Ryu, C. K.; Palke, W. E.; Ford, P. C. Ab Initio Studies of the Copper(I) Tetramers $Cu_4X_4L_4$ (X = I, Br, Cl). Effects of Cluster Structure and of Halide on Photophysical Properties. *Inorg. Chem.* **1994**, *33* (3), 561–566. https://doi.org/10.1021/ic00081a026.
(73) Raston, C. L.; White, A. H. Crystal Structure of the Copper(I) Iodide–Pyridine (1/1) Tetramer. *J. Chem. Soc., Dalt. Trans.* **1976**, *2*, 2153–2156. https://doi.org/10.1039/DT9760002153.
(74) Fersht, A. R.; Jencks, W. P. Acetylpyridinium Ion Intermediate in Pyridine-Catalyzed Hydrolysis and Acyl Transfer Reactions of Acetic Anhydride. Observation, Kinetics, Structure-Reactivity Correlations, and Effects of Concentrated Salt Solutions. *J. Am. Chem. Soc.* **1970**, *92* (18), 5432–5442. https://doi.org/10.1021/ja00721a023.
(75) Alcock, N. W.; Benton, D. J.; Moore, P. Kinetics of Series First-Order Reactions. Analysis of Spectrophotometric Data by the Method of Least Squares and an Ambiguity. *Trans. Faraday Soc.* **1970**, *66*, 2210. https://doi.org/10.1039/tf9706602210.
(76) Espenson, J. H. Chemical Kinetics and Reaction Mechanisms. McGraw-Hill Book Company, New York, NY. **1981**. ISBN 0-07-019667-2